Bulletin of the Seismological Society of America, Vol. 106, No. 6, pp. –, December 2016, doi: 10.1785/0120150233

Ⓔ

Moment Tensor Analysis of Very Shallow Sources

by Andrea Chiang, Douglas S. Dreger, Sean R. Ford, William R. Walter, and Seung-Hoon Yoo

Abstract An issue for moment tensor (MT) inversion of shallow seismic sources is that some components of the Green's functions have vanishing amplitudes at the free surface, which can result in bias in the MT solution. The effects of the free surface on the stability of the MT method become important as we continue to investigate and improve the capabilities of regional full MT inversion for source-type identification and discrimination. It is important to understand free-surface effects on discriminating shallow explosive sources for nuclear monitoring purposes. It may also be important in natural systems that have very shallow seismicity, such as volcanic and geothermal systems. We examine the effects of the free surface on the MT via synthetic testing and apply the MT-based discrimination method to three quarry blasts from the HUMMING ALBATROSS experiment. These shallow chemical explosions at ~10 m depth and recorded up to several kilometers distance represent rather severe source–station geometry in terms of free-surface effects. We show that the method is capable of recovering a predominantly explosive source mechanism, and the combined waveform and first-motion method enables the unique discrimination of these events. Recovering the design yield using seismic moment estimates from MT inversion remains challenging, but we can begin to put error bounds on our moment estimates using the network sensitivity solution technique (Ford *et al.*, 2010).

Online Material: Figures showing synthetic tests for a pure explosion and a composite source at local distances and table of moment tensor components.

Introduction

Waveform inversion to determine the seismic moment tensor (MT) is now a standard method for determining the source mechanism of natural and anthropogenic seismicity and can identify or discriminate different types of seismic sources. Such source-type identification is important for better understanding the physical processes of explosions and other anthropogenic events as well as earthquakes from geothermal (Guilhem *et al.*, 2014) and volcanic environments (Templeton and Dreger, 2006; Minson *et al.*, 2007) and from oil and gas operations (McNamara *et al.*, 2015). For the nuclear explosion discrimination problem the uncertainty in a given solution is as important as the best-fitting parameters, and it is therefore necessary to fully understand bias in source inversions. An issue for MT analysis of shallow seismic sources that are effectively at the free surface (depth is shallow compared to the modeled wavelength) is the indeterminacy of the M_{xz} and M_{yz} components of the MT. The vanishing traction at the free surface implies that the amplitudes excited by the M_{xz} and M_{yz} components, a diagonal MT with the ratio $\lambda : \lambda : (\lambda + \mu)$, and the displacement derivatives must vanish (Julian *et al.*, 1998). λ and μ are the Lamé constants. M_{xz} and M_{yz} correspond to a vertical dip-slip (DS) fault, and the diagonal tensor corresponds to a horizontal tensile fault which has an isotropic component.

The free-surface effect was noted in a study on fundamental Love and Rayleigh waves for nuclear explosions and associated tectonic release (Given and Mellman, 1986). The insensitivity of the Green's functions (GFs) to some components of the MT affects the stability of the recovered source mechanism (Bukchin *et al.*, 2010), and this problem becomes increasingly important as we continue to investigate and improve the capabilities of regional full waveform MT inversion for source-type identification and discrimination. It is important to understand its effects for discriminating shallow explosive sources for nuclear monitoring but could also be important in natural systems that have shallow seismicity, such as volcanic environments and geothermal systems, and other man-made shallow seismicity related to anthropogenic activities, such as hydraulic fracturing and mining.

To investigate the potential issues that could arise in the estimation of MTs for shallow sources, we perform a series of synthetic tests to document and understand the effects of the free surface on the total seismic moment, isotropic seismic moment, and the source mechanism for shallow sources in an

elastic medium. We evaluate the sensitivity of the MT solutions as a function of source depth, data quality, and velocity model. Based on what we learned from the synthetic studies, we applied the MT method to three quarry blasts from the HUMMING ALBATROSS experiment. The experiment was conducted in the eastern United States to acquire and study seismic and acoustic amplitude measurements from explosions in granite and under various confinement conditions. These small chemical explosions are ~10 m deep and are recorded at up to several kilometer distances. Therefore, the data represent rather severe source–station geometry in terms of free-surface effects. We show that the combined method utilizing both complete seismic waveforms and *P*-wave first-motion polarities is able to obtain robust full MT solutions that are composed predominantly of an isotropic or explosive component. However, unlike the synthetic studies, yield estimation using the real quarry blast MT inversion results remains challenging.

Methods

The seismic MT consists of nine force couples that represent the equivalent body forces for seismic sources of different geometries (Jost and Herrmann, 1989). Because of conservation of angular momentum, the nine couples reduce to six independent couples parameterized as the MT elements. The data (e.g., displacement waveforms) are represented by the convolution of GFs for a given Earth model, the source time function, and the MT elements. Because relatively long-period waves are used in the inversion, we assume that the source time function is an impulse. We obtain the individual MT elements by inverting the three-component, complete waveform data using a time-domain, generalized least-squares inversion (Minson and Dreger, 2008), and the goodness of fit between the data and synthetics is measured by the variance reduction (VR):

$$\mathrm{VR} = \left(1 - \frac{\sum_i w_i (d_i - s_i)^2}{\sum_i w_i d_i^2}\right) \times 100, \tag{1}$$

in which d is the data, s is the synthetic waveforms, and w is the inverse distance weighting at each station i. Because the data are linear combinations of the GFs weighted by their associated MT elements, one major source of error in the inverted MT solution comes from the assumed velocity model. A well-calibrated velocity model is important to obtain robust estimates of the source parameters. For HUMMING ALBATROSS, we used the 1D velocity model by Saikia *et al.* (1990) computed from *Rg*-wave dispersion and calculated the GFs using frequency–wavenumber integration (Wang and Herrmann, 1980; Herrmann and Wang, 1985; Herrmann, 2013). The inversion method also allows for small time shifts between the data and GFs to compensate for uncertainties in origin time, location, and velocity structure. To properly account for non-double-couple (non-DC) radiation, we used the Bowers and Hudson (1999) formulation to calculate the moment magnitude. The MT is decomposed into isotropic (ISO), DC, and compensated linear vector dipole (CLVD) based on the Bowers and Hudson (1999) total seismic moment, and the deviatroic moment is then decomposed using the scheme described in Jost and Herrmann (1989), in which the DC and CLVD share the same P and T axes (Knopoff and Randall, 1970).

To assess the uncertainties in the MT inversion and avoid the need to decide on a particular MT decomposition scheme, we examine the MT solution in terms of the maximum fit surface called Network Sensitivity Solutions (NSSs; Ford *et al.*, 2010). The NSS compares the goodness of fit between data and synthetic waveforms for a suite of full MT solutions in source-type space (Hudson *et al.*, 1989; Tape and Tape, 2012a,b; Vavryčuk, 2015) and generates a distribution of VR for a given station configuration, Earth model, and period range. Ford *et al.* (2010) assembled the population of MTs from a distribution of randomly generated eigenvalues and orthonormal eigenvectors in source-type space, but instead of the original forward approach we implemented the iterative damped least-squares inversion scheme by Nayak and Dreger (2015) to compute the best-fitting MT for each source type. This method significantly reduces the computation time and recovers a true maximum fit surface in the source-type space. In essence, the source-type diagram is a graphical representation of the full MT eigenvalues with two key parameters γ and δ, which are the longitude and latitude of a fundamental lune on the unit sphere:

$$\tan\gamma = \frac{-\lambda_1 + 2\lambda_2 + \lambda_3}{\sqrt{3}(\lambda_1 - \lambda_3)}, \tag{2a}$$

$$\cos\beta = \frac{\lambda_1 + \lambda_2 + \lambda_3}{\sqrt{3(\lambda_1^2 + \lambda_2^2 + \lambda_3^2)}}, \tag{2b}$$

$$\delta = \frac{\pi}{2} - \beta, \tag{2c}$$

(Tape and Tape, 2012a,b). β is the colatitude, and λ_{1-3} are the eigenvalues of the full seismic MT, in which $\lambda_1 \geq \lambda_2 \geq \lambda_3$. Equation (2a) measures the deviation from a pure shear dislocation, and equations (2b) and (2c) describe the volume change. In this convention when $\delta = 0$ (no volume change), $\gamma = 0$ describes a pure DC source, and $\pm\pi/6$ describes a pure CLVD source. When there is volume change, $\gamma = 0$ and $\delta = \pm\pi/2$ represent spherical explosion ($+V$) and implosion ($-V$), respectively. The distribution of MTs assembled to compute the NSS comes from a grid on the fundamental lune where each grid point represents a unique set of normalized eigenvalues. The inversion is performed at each grid point to obtain the best-fitting eigenvector and moment scale factor yielding the maximum fit surface, or NSS, on the fundamental lune. The NSS is shown as a contour map where each contour

represents the population of best-fitting MT solutions that have VR equal and above a certain threshold. In descending order, the contours map out the solutions that have VRs of 98%, 95%, 90%, 80%, 70%, 60%, and 50% of the maximum VR in the NSS population. From the NSS of a given event we can determine whether or not the best-fitting full MT solution from the inversion is well resolved to make useful interpretations about the source. Understanding the relative contributions of the different MT elements provides insights into the complex source processes of explosions as well as other seismic events. This representation of the seismic source has been shown to result in separate populations for explosions, underground cavity collapse, and earthquakes (Dreger *et al.*, 2008; Ford *et al.*, 2008, 2009a,b; Chiang *et al.*, 2014), enabling discrimination capability.

In addition to long-period waveform data, we include *P*-wave first-motion polarities in the NSS calculations as additional constraints (Chiang *et al.*, 2014; Guilhem *et al.*, 2014). The joint inversion finds the MT solutions that best fit both the complete waveform data and the *P*-wave first-motion polarities; the theory for the approach is given in Nayak and Dreger (2015). Similar to comparing synthetic waveforms to data, we compare the theoretical *P*-wave first-motion polarities against the observed polarities. We assign -1 for downward motion and $+1$ for upward motion, and each observed polarity is weighted by the quality of the pick. The first-motion VR is calculated as

$$\mathrm{VR} = \left(1 - \frac{\sum w_i(\mathrm{Pol}_{\mathrm{obs}} - \mathrm{Pol}_{\mathrm{synth}})^2}{\sum w_i \mathrm{Pol}_{\mathrm{obs}}^2}\right) \times 100. \qquad (3)$$

The combined VR is computed by weighing the two data sets equally. Incorporating the first-motion data proves to be a powerful tool in reducing solution uncertainties. Constraints from first motion can reduce uncertainties due to the theoretical ISO–CLVD trade-off (Ford *et al.*, 2012; Chiang *et al.*, 2014), sparse station coverage (Chiang *et al.*, 2014), possible complexities in earthquake ruptures in geothermal environments (Guilhem *et al.*, 2014), and, as illustrated later in this study, free-surface effects at shallow depths. We find that the additional polarity constraints assist by uniquely discriminating the events as predominantly explosive and greatly enhance the discriminatory power of the MT-based method.

Green's Functions near the Free Surface

We generate the 10 fundamental fault GFs at a distance of 100 km from the source and with source depths ranging from 0.2 to 1.2 km, and apply an acausal band-pass Butterworth filter at 10–50 s to filter the GFs. As shown in Figure 1a, we see a strong source depth dependency on the vertical DS fundamental GFs associated with the M_{xz} and M_{yz} elements for all three components: vertical (ZDS), radial (RDS), and transverse (TDS) in which there is a systematic reduction in displacement amplitude with decreasing source depth. The averaged Fourier spectral amplitude shows a linear relationship between the source depth and DS waveform amplitudes (Fig. 1b). In contrast, the vertical strike-slip GFs for all three components (ZSS, RSS, and TSS) and the explosion GFs for the vertical and radial components (ZEX and REX) show little to no variation in amplitude and waveform with respect to decreasing source depth. The vertical and radial 45° DS GFs (ZDD and RDD) show variations in amplitude as well, due to the constructive and destructive interference of waves interacting with the free surface. Although the wave interference appears minor in the 10–50 s period passband (Fig. 1a), it is more pronounced in the unfiltered displacement GFs.

Because the GFs are not sensitive to some components of the MT, the inversion may not resolve these components, such as M_{xz} and M_{yz} as well as the isotropic components M_{xx}, M_{yy}, and M_{zz}. It is important to note however that although there are strong effects on the GF amplitude, the waveforms remain similar, and there is little effect on the phase of the waveforms of these components. The systematic behavior of the GF suggests that it may be possible to scale the isotropic moment (M_{I}) by the changes in GF amplitude with respect to depth to recover the correct moment, enabling a more robust estimate of the explosive yield. Because the ability to resolve seismic waveforms at the free surface depends on the velocity model, period range, station configuration, and background noise level, it is necessary to understand the behavior of the MT inversion for each particular monitoring scenario to correct for bias in the seismic moment. Poor station coverage and low signal-to-noise ratio (SNR) will decrease the method's ability to fit the observed waveforms and resolve the problematic MT components.

In the synthetic study, we examine the ability to recover the correct MT elements by generating a suite of velocity models derived from a 1D western U.S. reference velocity model (Song *et al.*, 1996). We choose this particular model as a reference because it was used to model the Nevada test site (NTS) explosions in Ford *et al.* (2009b). We generated the suite of models by splitting the top 2.5-km-thick layer in the reference model into two separate layers. We systematically adjust the thickness and velocity of the two new layers (Fig. 2), but constrain the perturbations of the two parameters (velocity and layer thickness) to maintain the same vertical travel time as the reference model to generate different but comparable velocity models and to minimize travel-time differences. For each 1D model, we generate displacement GFs at regional distances between 100 and 400 km, with source depths ranging from 0.2 to 3.5 km. Using the same set of GFs, we generate two types of synthetic data with different source mechanisms: (1) a pure explosion case (EXP) and (2) a composite source case (DC and EXP) with a DC to EXP ratio of 2:3. We compute the synthetic data following the expressions from Minson and Dreger (2008) and add random Gaussian white noise. We scale the amplitude of the random noise for a given SNR using the following equation:

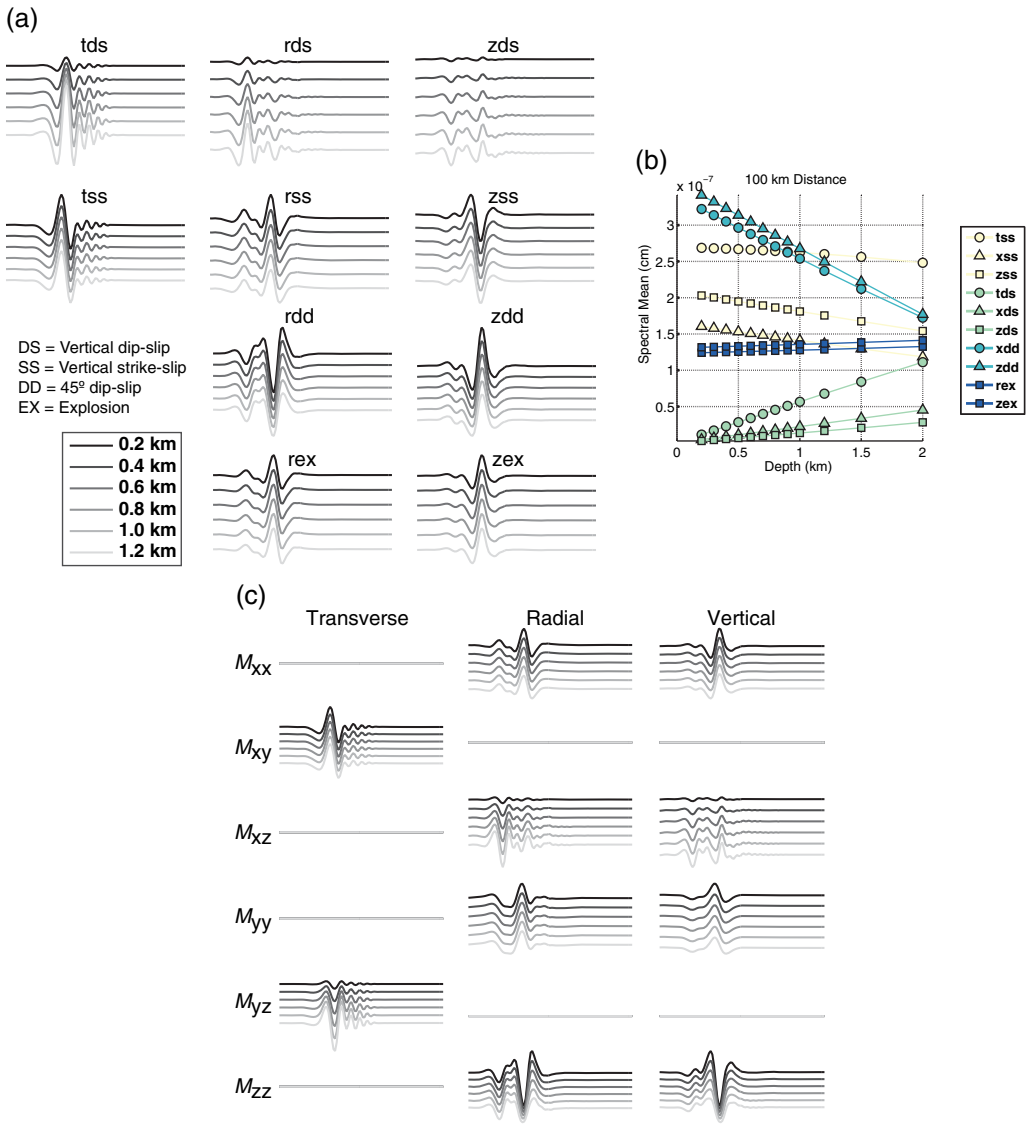

Figure 1. (a) Theoretical Green's functions (GFs) computed using the Song *et al.* (1996) 1D western U.S. velocity model and filtered between 10 and 50 s period. The waveforms are in displacement (cm) and each component, from top to bottom, is at 0.2, 0.4, 0.6, 0.8, 1.0, and 1.2-km source depths. (b) Averaged spectral displacement amplitudes between 10 and 50 s for the 10 fundamental GFs. (c) Moment tensor (MT) elements computed using the same velocity model from (a) and filtered between 10 and 50 s period. The color version of this figure is available only in the electronic edition.

$$\mathrm{SNR} = 20\log_{10}\left(\frac{\mathrm{rms}_{\mathrm{signal}}}{C_{\mathrm{noise}}\mathrm{rms}_{\mathrm{noise}}}\right). \qquad (4)$$

The scaling factor C_{noise} is calculated for a given SNR using the root mean square (rms) amplitudes of the signal and noise, then the noise-included data and GFs are band-pass filtered between 10 and 50 s using an acausal Butterworth filter. To model after real-life monitoring capabilities, we used an SNR of 10 but also tested different SNRs. We implemented a four-station coverage for the MT inversion, consisting of source-to-receiver distances at 100, 200, 300, and 400 km and at azimuths of 0°, 83°, 202°, and 301°, respectively.

In the first test, we keep the source depths of the synthetic data and the GFs used in the inversion the same to isolate the effect of the free surface for shallow depth of burial. Of the 59 velocity models tested, the full MT inversion successfully recovers the correct mechanism for both the pure explosion case and the composite case over the targeted depth range (< 1 km) for nuclear explosions as well as at deeper depths. Given the same filter parameters and station configuration, models that have a thick continuous layer generally have larger deviations in the moment estimates, whereas the more gradient-like models show little to no change. Figure 3 shows the sensitivity of total and isotropic scalar moment with respect to source depth. At the shallowest depths (< 0.5 km), for the pure explosion case the M_{I} estimates all fall within about 10% of the input values (Fig. 3a), whereas the total moment varies even less. The composite case exhibits greater

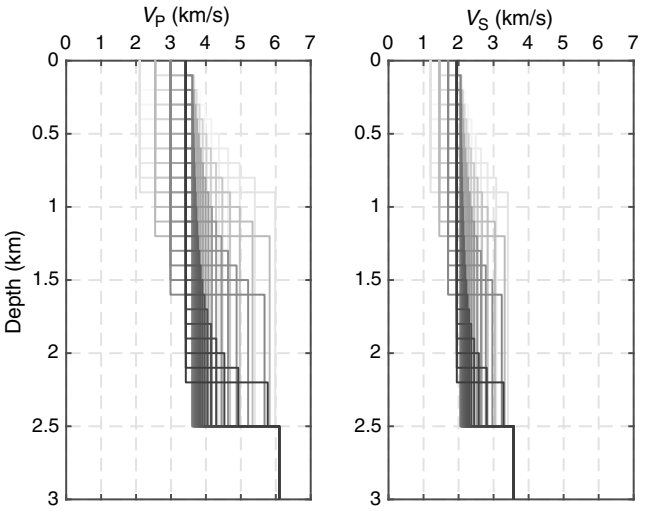

Figure 2. Velocity models derived from the Song *et al.* (1996) 1D model by keeping the top 2.5-km vertical travel-time constant. The model parameters are the same below 2.5 km depth.

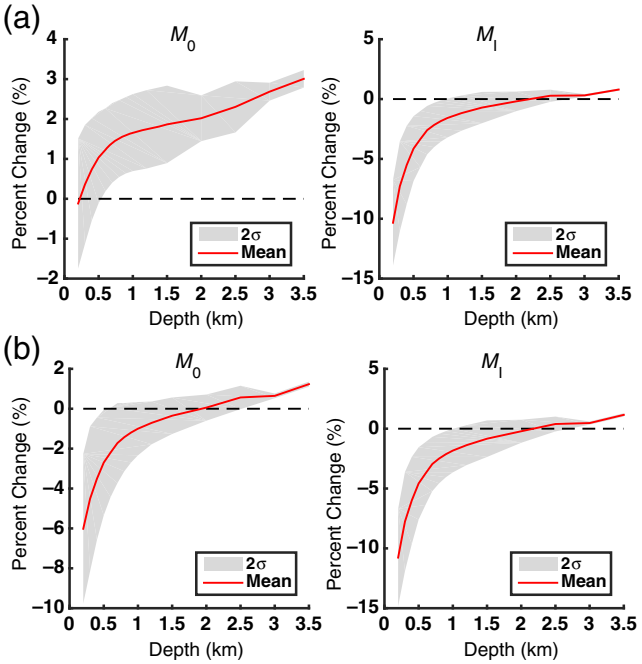

Figure 3. Isotropic moment (M_I) and total seismic moment (M_0) percent change for (a) a pure explosion source and (b) a composite explosion plus double-couple (DC) source plotted as functions of source depth. The average value of all 59 models is the solid line; the shaded region is 2σ from the mean; and the dashed line represents no deviation from the input seismic moments. The color version of this figure is available only in the electronic edition.

deviations from the input value at the shallowest source depths; however, all moment estimates are within about 20% of the input values (Fig. 3b). In general, the seismic moment estimates approach the correct value as the source depth increases. The M_{zz} component is not as well constrained, thus affecting the method's ability to resolve M_I. In most cases, free surface vanishing traction has little effect on recovering the correct mechanism for models with a shallow velocity gradient. However, as the noise level increases, the bias in the seismic moment and mechanism also increases. The key observation from the synthetic tests is that the bias in the recovered moment and source mechanism of very shallow sources depend on various factors, including the velocity model.

In practice, when we perform MT inversions, the source depth is also tested because we do not know the true source depth. Thus, we also looked at synthetic comparisons where we fixed the source depth and tested the full suite of GF depths. Results at source depths 0.5 and 3.0 km are shown in Figure 4. In this synthetic test, the deviation from the true seismic moment is much greater, due to errors from incorrect source depth, and the percent change in total and isotropic moment decreases as the GF depths approach the correct value. For the two source depths shown, the mean percent changes in moments are similar, but the spreads are different. For example, when source depth is at 0.5 km, the change in isotropic moment away from the true source depth encompasses a much wider range compared to the case with source depth fixed at 3.0 km. The change in VR is most prominent at a source depth of 3.0 km because a layer boundary exists at 2.5 km for all the velocity models. The set up for the synthetic test is based on regional monitoring conditions reflective of current nuclear monitoring capabilities. Given the difference in scale for the HUMMING ALBATROSS experiment, we repeat the same analysis at source depths between 0.01 and 1.2 km, recording distances up to 4 km and filter passband between 0.5 and 2 s. The results at the correct GF depth (Ⓔ Fig. S1) and variable GF depth (Ⓔ Fig. S2) are available in the electronic supplement to this article. In general, the local distance observations are similar to the regional case, but the deviations from the true moment are larger and have higher variability at these very shallow depths (Ⓔ Fig. S1). The larger variability is likely due to greater sensitivity to the velocity structure. For the case with variable GF depth (Ⓔ Fig. S2), VR decreases and the moment deviates from the true value more quickly as the GF deviates from the correct source depth. The more rapid changes are due to short-period waves being more sensitive to the changes in source depth.

HUMMING ALBATROSS

The synthetic tests show that although the low sensitivity of the GF at the free surface can affect the method's ability to resolve the moment at shallow depths, the impact on the recoverability of the source mechanism is much less. To further evaluate the performance of the MT method for shallowly buried sources, we apply the method to data from the HUMMING ALBATROSS series. The data sets consist of 26 broadband, strong-motion, and short-period seismic recordings (Fig. 5). The chemical explosions are detonated inside boreholes at very shallow depths (< 20 m) and recorded at stations up to several kilometers. We apply the MT-based discrimination method to three of the five chemical explosions

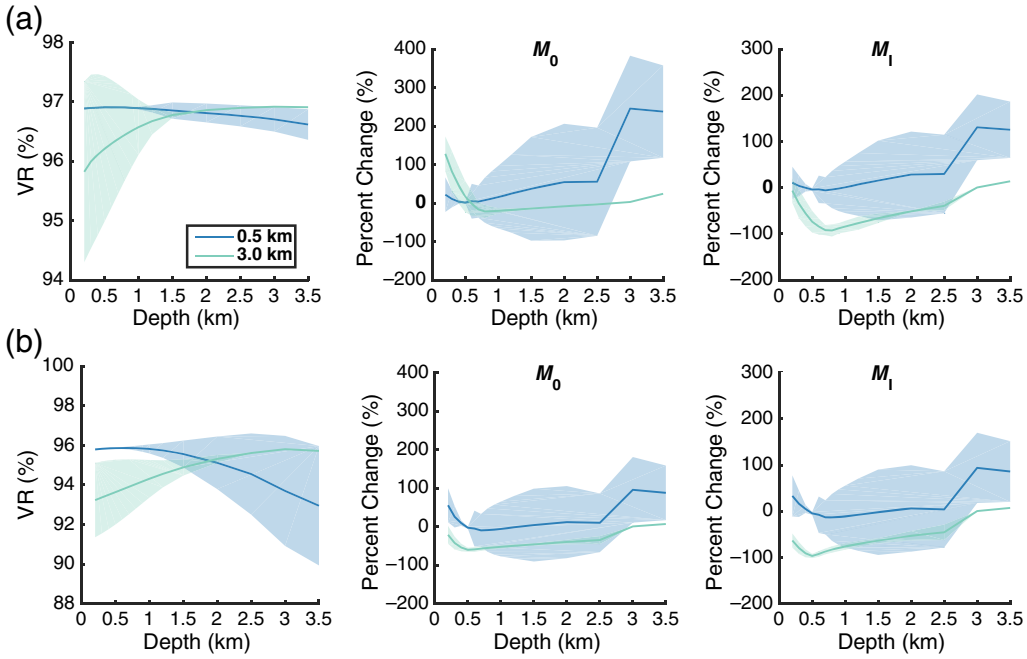

Figure 4. Source depth sensitivity analysis in which source depth is fixed while the full suite of GF depths (x axis) is tested. Comparisons of variance reduction (VR), total moment (M_0) percent change, and isotropic moment (M_I) percent change as a function of varying GF depth are shown for (a) a pure explosion source and (b) a composite source. The solid lines are the average values of all 59 models, and the shaded regions are 2σ from the mean. The color version of this figure is available only in the electronic edition.

(production, 800, and 400). The two smallest events in the series have poor SNR below 3 Hz; and we cannot estimate the source parameters with high confidence. Weston Geophysical Corp. provided the instrument corrected velocity and acceleration data for HUMMING ALBATROSS, and we prepare the velocity waveforms for source analysis by rotating the horizontal recordings to radial and transverse components, and band-pass filtered the data and GFs with an acausal Butterworth filter. Depending on the instrument response and data quality, the band-pass filter applied to each station ranges between 0.4 and 1.25 s. Table 1 lists the source depth and filter corners used, and the moment magnitude (M_w), M_I, and waveform fits (VR) from time-domain full MT inversions, whereas the MT elements are listed in Ⓔ Table S1.

Following the results of Ford *et al.* (2012) and Chiang *et al.* (2014), we utilize full waveform data from broadband and/or short-period stations for the time-domain waveform inversion and include both waveform and *P*-wave first-motion polarities from all 26 stations into our source-type uncertainty analysis. We present results from the MT sensitivity analysis both as a function of depth and period for the largest, delayed-fire production shot.

The time-domain MT inversion yields similar results for all three explosions in which the full MT solutions all have relatively large isotropic components that are approximately between 40% and 50% of the total seismic moment, and the deviatoric inversions all result in vertical DS-like mechanisms (Fig. 6). The deviatoric solutions are thus dominated by the M_{xz} and M_{yz} components, which as shown in Figure 1c, the TDS, RDS, and ZDS GFs show a marked reduction in amplitude with decreasing source depth. An example of the waveform fits and MT solutions for the production shot is shown in Figure 7. All three explosions have strong shear-wave energy in the transverse component, and many of those components have amplitudes comparable to Rayleigh waves on the vertical component. We avoid using stations in the direction of the free face (quarry cliff) for the production shot because of spallation at the cliff face. For shot 800, we tried a combination of stations with and without those in the direction of the free face and found the MT solutions to be very similar.

The production shot source parameter uncertainties using only seismic waveforms show the best-fitting mechanisms are mostly isotropic (Fig. 8a). The source parameters are well constrained for solutions with VRs equal to and above 95% of the maximum VR, but if we relax the threshold down to 90% of the maximum VR, the population of well-fitted solutions extends across the DC/deviatoric line. Previous NSS studies of nuclear explosions have shown trade-offs between ISO ($+V$) and $-$CLVD mechanisms but generally not between ISO and DC mechanisms (Ford *et al.*, 2012; Chiang *et al.*, 2014). A combination of strong Love waves and free-surface effects most likely contributed to this apparent ISO–DC trade-off and it is especially pronounced for the two smaller shots. To increase the confidence in our MT solutions, we bring in constraints from *P*-wave first-motion polarities. Unlike previous studies (e.g., Ford *et al.*, 2012; Chiang *et al.*, 2014), we have relatively good azimuthal coverage for the first-motion observations that sampled the majority of the focal sphere, significantly reducing the NSS to a predominantly explosive mechanism (Fig. 8b). The best solutions from the combined

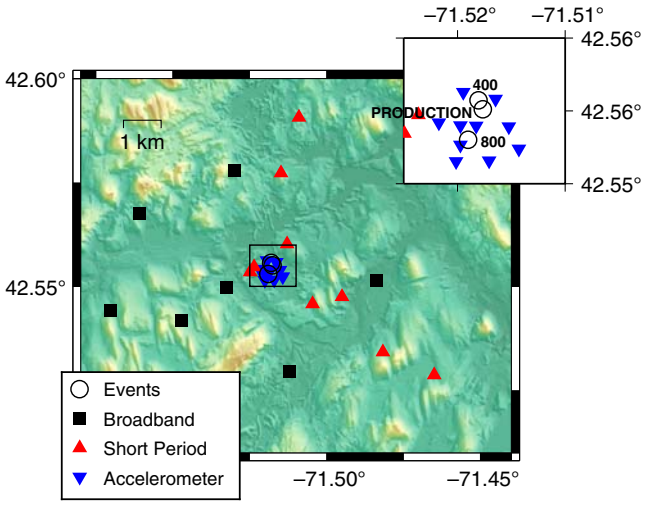

Figure 5. Event and station locations for the HUMMING ALBATROSS experiment. The seismic array includes broadband instruments (squares), short-period sensors (triangles), and accelerometers (inverted triangles). Three (production, 800, and 400) of the five chemical explosions (circles) were studied, and the background represents the local topography. The color version of this figure is available only in the electronic edition.

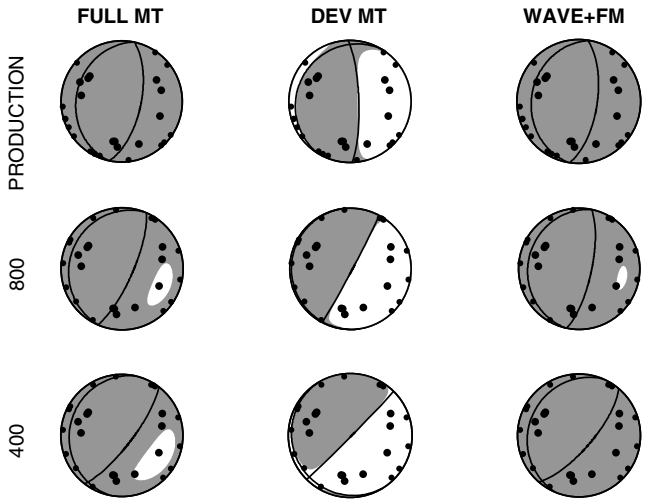

Figure 6. HUMMING ALBATROSS MT solutions from time-domain full (FULL) and deviatoric (DEV) inversion and the best solution from combined waveform and *P*-wave first-motion (filled circles) network sensitivity solutions (NSSs; WAVE + FM). All polarities are up.

NSS are similar to the solutions from the waveform-only inversions (Fig. 6), in which MT solutions that deviate away from a theoretical opening crack do not fit the observed polarities. NSSs for shots 800 and 400 show similar behaviors, namely the ISO–DC trade-off using only waveforms, and a well-constrained solution when combining both waveform (body and surface waves) and *P*-wave first-motion polarities. We also present an example of a first-motion only NSS (Fig. 8c). The maximum fit surface using only polarity data is extensive; therefore, first motions alone are not sufficient for event source-type discrimination.

Given the period range and source–receiver distance, the MT inversion is not very sensitive to source depths shallower than ~100 m. We estimate source depth sensitivity by looking at the VR as a function of source depth and observe that the deviatoric VR drops sharply starting around 100 m, whereas the full VR shows a more gradual decrease in VR. If we have no prior knowledge on source depth, the sensitivity analysis shows we can constrain the depth to be shallower than ~100 m, indicative of possible man-made seismicity because natural earthquakes rarely occur at these depths. Although we do not have much sensitivity at the very shallow depths, the mechanisms remain stable and predominantly explosive at the borehole depths (Fig. 9a,b), where the explosions are detonated. We start to see a trade-off between the mechanism and incorrect source depth at around 100 m for the production shot and at around 50 m for 800 and 400; however, the combined waveform and first-motion inversion eliminates this trade-off. Because we know the depth of the borehole where the explosions are detonated, we focus on the behavior of seismic moment at depths less than and equal to 20 m. Because of free-surface effects, the total and isotropic moment increases as source depth decreases (Fig. 9c,d), and the increases in seismic moments are controlled by changes in the M_{zz} and M_{yz} components (Fig. 9d), which we anticipated to be strongly influenced by the free surface. The behavior of the MT solution as a function of depth is similar for shots 800 and 400, although the free-surface effects are more pronounced at the shallowest depths, where the full MT solutions become vertical DS due to a greater increase in moment from the M_{yz} component.

The Earth becomes very heterogeneous at short periods where the smoothed 1D model is no longer adequate in characterizing the complexities in short-period wave propagation between the source and receiver. Therefore, the reason for utilizing long-period waveform data is to minimize the bias

Table 1
Moment Tensor Solution and Yield

Event	Centroid Depth (m)	Inversion Depth (m)	Filter (s)	M_w	M_1 (N·m)	VR (%)	Estimated Yield (tons)	Design Yield (tons)
Production	Varied	11	0.5–1.25	2.5	3.25×10^{12}	70	29	9.22
800	9	9	0.5–0.83	1.9	3.36×10^{11}	72	3.0	0.357
400	11	11	0.4–1	1.6	9.91×10^{10}	67	0.9	0.182

VR, variance reduction.

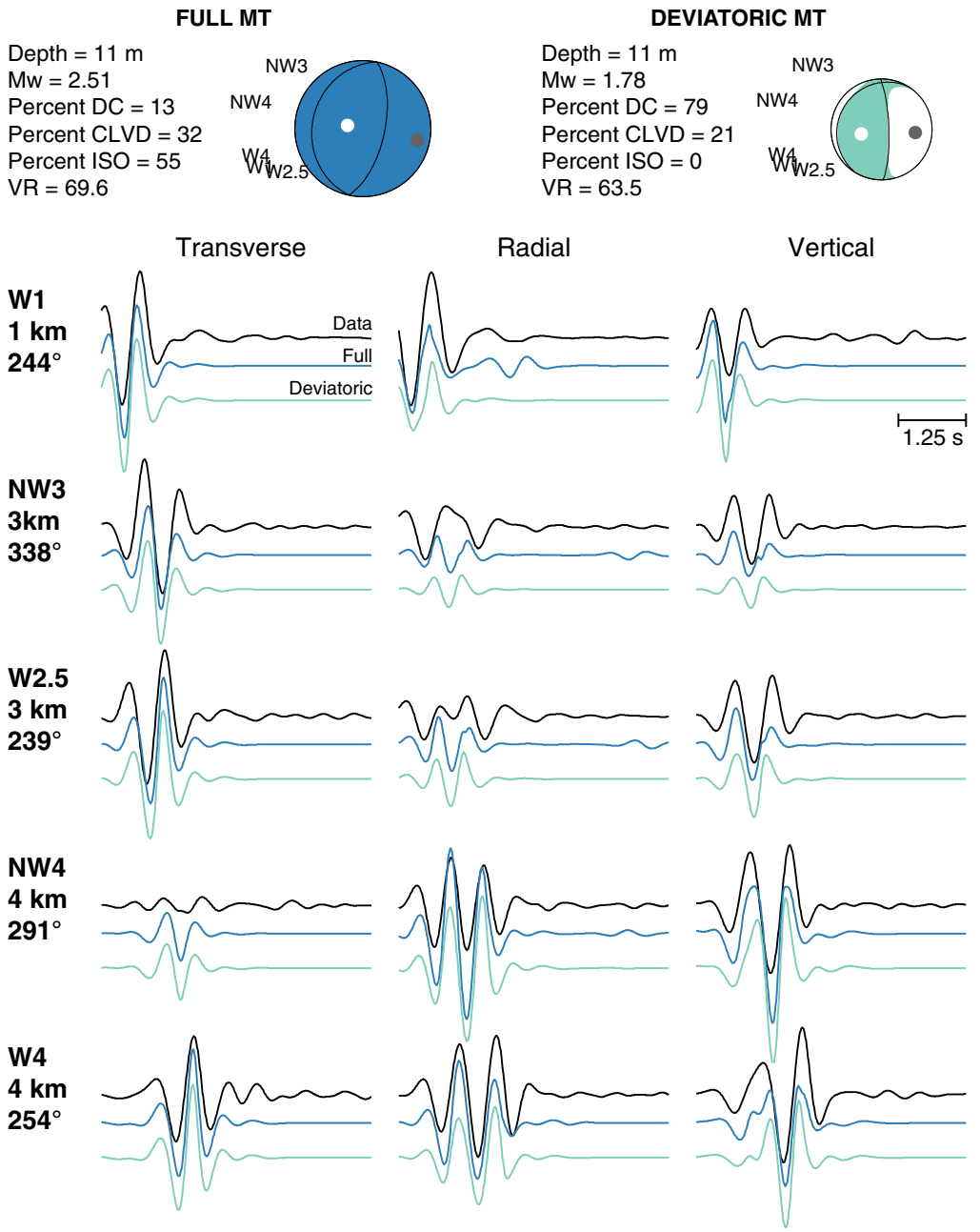

Figure 7. Production shot focal mechanisms and waveform fits from full and deviatoric MT inversions. The color version of this figure is available only in the electronic edition.

from unaccounted velocity structures. However, the challenge for MT inversion at these very shallow depths for the HUMMING ALBATROSS data is that the free-surface effect increases not only with decreasing source depth but also at longer periods. The production shot has relatively good SNR at periods up to 2.5 s, but if we fix the source depth to 11 m and look at the free-surface effects on the inversion as a function of filter passband, we see the solutions become vertical DS at longer periods (Fig. 10a,b). The total moment increases (Fig. 10c) as we go toward longer periods due to rapidly increasing contributions from the M_{xz} and M_{yz} components (Fig. 10d). Hence finding the optimal filter passband that minimizes both the effects of the velocity structure at short periods and the free surface at long periods is especially important and potentially challenging for MT analysis of shallow sources. However, it is important to note again that by combining the first motions with the waveforms, this issue is eliminated or at least suppressed.

Yield Estimates

Far-field amplitude is linearly related to yield, so the relationship between magnitude and yield can be described by the following equation:

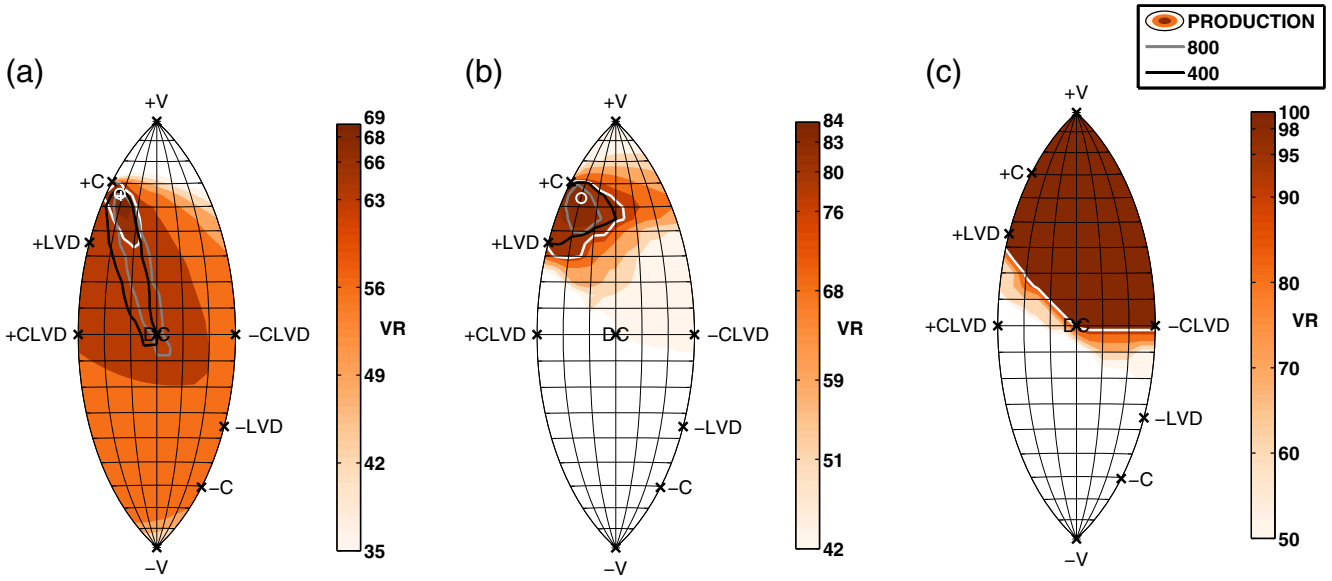

Figure 8. NSSs using (a) waveforms, (b) waveform and *P*-wave first motions, and (c) *P*-wave first motions. The best MT solutions from NSS (circle) are plotted in (a) and (b), and MT from time-domain waveform inversion (plus) is plotted in (a). Production shot NSS are plotted as shaded contours, and the contours are populations of solutions with normalized VR $\geq$ 95%, relative to the maximum VR for each shot. The color version of this figure is available only in the electronic edition.

$$M = A \log_{10} Y + C, \tag{5}$$

in which M is the seismic magnitude, Y is the yield in kilotons, and A and C are constants that depend on the magnitude measurement used. C may also include additional corrections to account for differences in the source medium that are independent of the yield. Empirical relationships to estimate yield have been developed using body-wave magnitudes (m_b) and surface-wave magnitudes (M_s) (e.g., Mueller and Murphy 1971; Murphy, 1977, 1996; Burger *et al.*, 1986) from past nuclear explosions with known yields. Given and Mellman (1986) and Ekström and Richards (1994) performed MT inversions on the Shagan River explosions from the former Soviet Union and explosions from the U.S. NTS and computed moment–yield relationships for those events. Yield estimation using M_I from MT inversions can be challenging, due to difficulties assessing the contributions from the isotropic and the nonisotropic radiation of the source as discussed in Stevens and Murphy (2001) and damage as discussed in Patton (2012), as well as due to free-surface effects at shallow depths. However, as demonstrated in Ford *et al.* (2012) and Chiang *et al.* (2014) and the previous sections of this article, source-type analysis (NSS) and the combination of waveform and first-motion data can help to better constrain the isotropic radiation of the MT.

We calculated the yields for HUMMING ALBATROSS using the MT results at the reported centroid depths, and the M_I-yield relationship $M_I = \log_{10} Y + 14.05$ from Stevens and Murphy (2001). The empirical relationship is derived from previously published MT inversion results and announced yields or estimated yields from Shagan and NTS explosions (Fig. 11a). To use the Stevens and Murphy (2001) empirical relationship, we extrapolate the curve down to very low values of yield and isotropic moment where the relationship was not originally defined. Because the empirical relationship is derived from nuclear explosions, differences in the seismic coupling efficacy between nuclear and chemical explosions (Murphy, 1996) can also bias our yield estimates. We present our yield estimates and the design yields in Table 1. The MT inversion at shallow depth overestimates the yields for all three explosions; the estimated values are approximately three times, eight times, and five times greater than the design yield for the production shot, 800, and 400, respectively. However, from our combined NSS analysis we can estimate the errors associated with our MT solutions. We choose a population of MT solutions with normalized VRs $\geq$ 90% and computed the mean and 2σ from the mean. For the production shot, the mean is very close to the Stevens and Murphy (2001) scaling, and for the two smaller shots the lower error bounds overlaps with the empirical scaling.

From our synthetic studies on the effects of the free surface at regional distances, we observe that the recovered mechanism is less sensitive to the source depth, but there can be bias in the moment due to the low sensitivity of the GF near the surface. In case of real observations, nonlinear response of the medium for shallow sources can also contribute to the bias in moment. Although the deviations from the true moment are all within 20% from our synthetic tests, the amount of deviation also depends on station coverage, period passband, and SNR. Additional synthetic tests on varying the station coverage, period range, and noise level suggest that, although the amount of bias in M_I varies, the asymptotic behavior as a function of depth remains similar and that the recovered M_I approaches the true value as the source depth

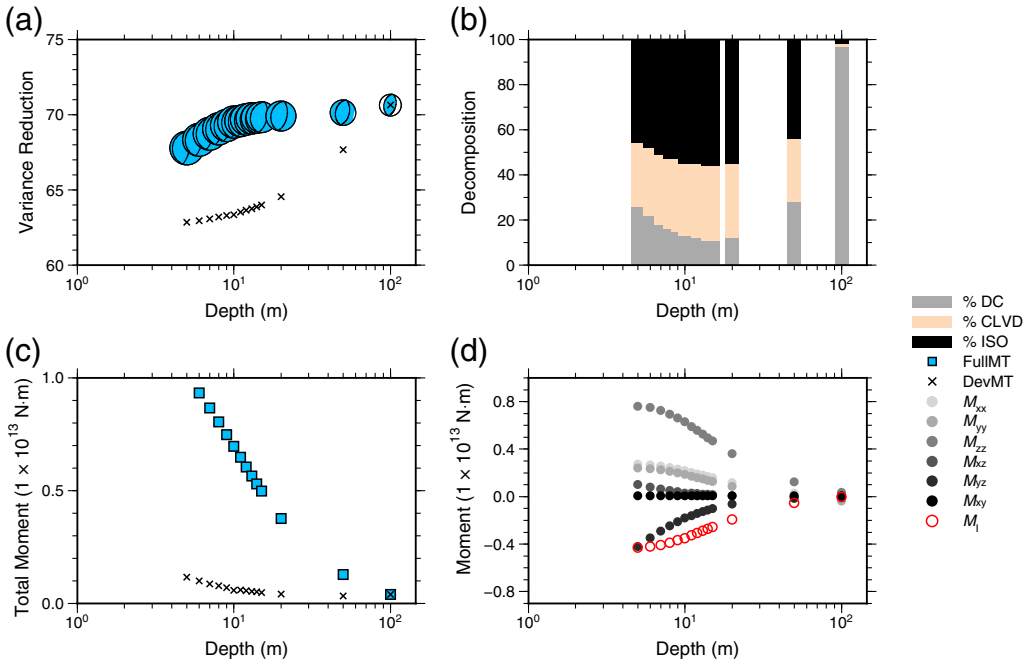

Figure 9. Production shot MT solutions as a function source depth and using only waveform data. (a) VR from full MT inversion (focal mechanism plots) and deviatoric (MT) inversion (crosses), (b) full MT decomposition where the shaded bars are the percent DC, compensated linear vector dipole (CLVD), and isotropic (ISO) components, (c) total moment from full inversion (squares) and deviatoric inversion (crosses), and (d) MT elements (filled circles) and isotropic moment (open circles). The color version of this figure is available only in the electronic edition.

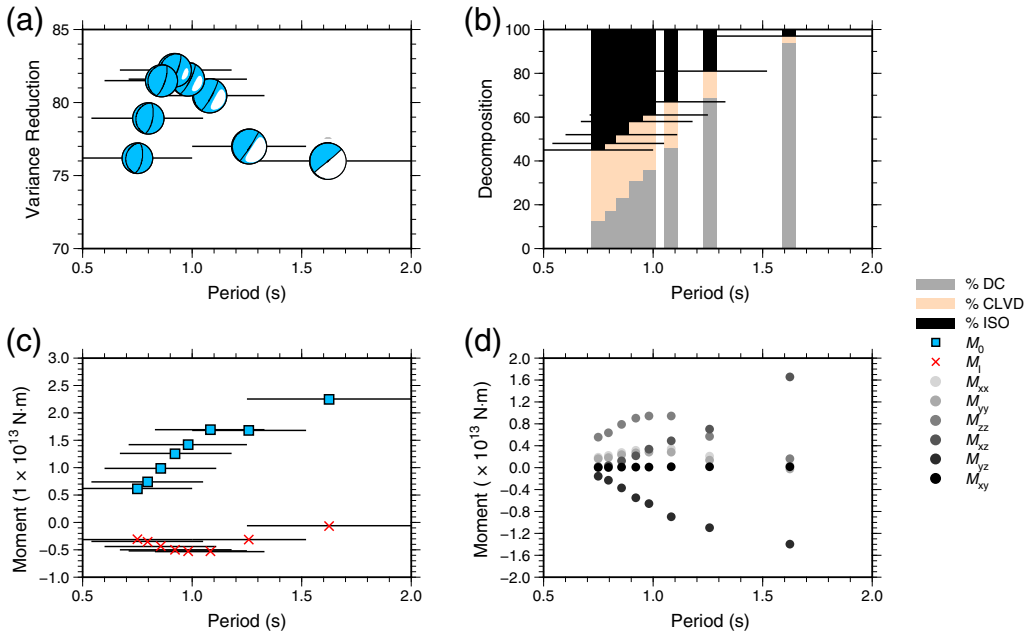

Figure 10. Production shot full MT solutions as a function of filter passband and using only waveform data. (a) VR and focal mechanism, (b) MT decomposition, (c) total moment (squares) and isotropic moment (crosses), and (d) MT elements (filled circles). Horizontal lines in (a)–(c) specify the filter passband used for each inversion at 11 m depth. The color version of this figure is available only in the electronic edition.

increases. Thus to minimize the free-surface effects it may be possible to invert for the source parameters at a deeper depth where the synthetic tests show the M_I approaches the true value. Here, we investigate the possibility of recovering the correct yield by intentionally inverting for the source at a deeper depth.

We first perform similar synthetic tests for a pure explosion scenario using the production shot station configuration,

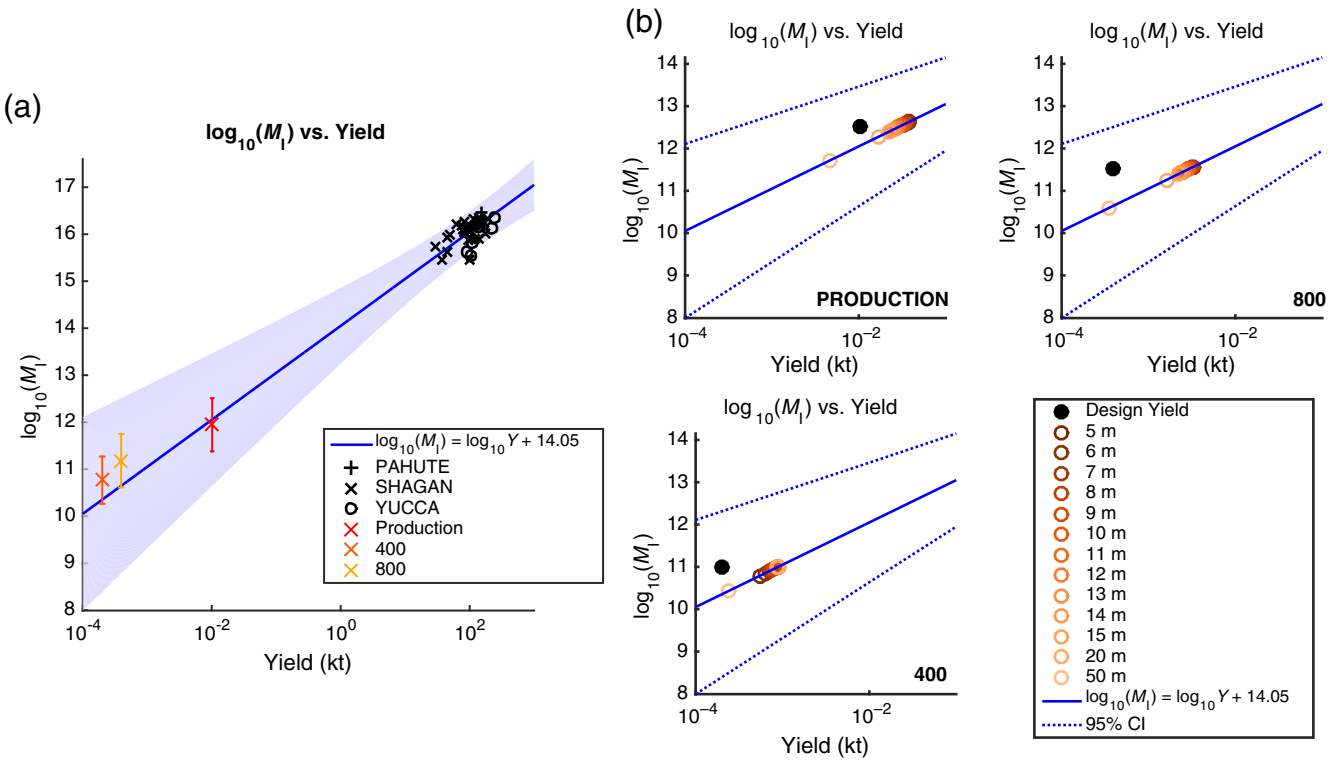

Figure 11. (a) Isotropic moment (M_I) versus yield (Y) for nuclear explosions from Stevens and Murphy (2001) and HUMMING ALBATROSS chemical explosions (production, 800, and 400). The solid line is the moment–yield scaling relation from Stevens and Murphy (2001), and the shaded regions are the 95% confidence bounds (CI). The mean M_I and error bars (2σ) for the three chemical shots are computed from a population of MTs with normalized VRs $\geq$ 90% in the combined NSS, as shown in Figure 8b. (b) Yields for production, 800, and 400 explosions, calculated using the empirical scaling relation by Stevens and Murphy (2001), and for M_I (at the reported centroid depth) from waveform MT inversion are plotted at various depths (open circles), as well as the design yield (filled circles). The moments are in newton meters·m and the yields in kilotons. The color version of this figure is available only in the electronic edition.

filter passband, and 1D velocity model to predict the depth range in which we can minimize both the effects from GF insensitivity and incorrect source depth. We fix the depth of the data but vary the depth of the GFs (as is done in practice when source depth is unknown or has large uncertainties) and found that the MT inversion is able to recover the correct focal mechanism and seismic moment at depths between 20 and 50 m. This is an idealized case with no time shift in the inversion, high SNR, and perfect knowledge of the Earth structure; the question remains whether this adjustment in the source depth can correctly estimate the yield from real explosions for which we have imperfect knowledge of the Earth structure.

In Figure 11b, the yield estimates for HUMMING ALBATROSS as a function of source depth are compared. In general, because M_I decreases as source depth increases, the estimated yield also decreases. Yields computed from M_I obtained at 20 and 50 m depth do agree with the design yield, but as noted previously we start to see trade-off between incorrect source depth and source mechanism around 50–100 m, where the MTs are no longer predominately explosive. Unlike the synthetic case, with real data when we introduce additional errors from incorrect source depth can have a greater impact on the recoverability of the mechanism, particularly for the smaller shots 800 and 400 for which we use short-period waveforms.

Discussion

Synthetic MT inversion tests show that although the low sensitivity of the GF near the free surface affects the MT inversion's ability to resolve the seismic moment at shallow depths, the impact on the recoverability of the source-type (explosion, DC, composite mechanism) is substantially less. This is illustrated by the successful discrimination of the NTS, Democratic People's Republic of Korea (DPRK), Soviet Joint Verification Experiment (JVE), Chinese Lop Nor (Ford *et al.*, 2009a,b, 2010; Chiang *et al.*, 2014), and HUMMING ALBATROSS events as explosions. However, the degree in which the free surface affects the seismic moment depends not only on the station geometry, noise levels, and filter passband but also on the velocity model. Free-surface effects are more pronounced when modeling longer wavelengths.

Nonisotropic radiation in the HUMMING ALBATROSS MT solution results from a combination of both the free-surface effect and the strong *SH* waves. *SH* and Love-wave generation from nuclear explosions (e.g., Ekström and Richards, 1994; Vavryčuk and Kim, 2014) and chemical explosions is not an uncommon observation, and a number of studies on quarry blasts suggest that the nonisotropic radiation results from spall of material from the quarry face (Goforth and Bonner, 1995; Bonner *et al.*, 1996) and the interaction of the wavefield with the severe topographic features of quarry benches (Barker *et al.*, 1993). McLaughlin *et al.*, (2004) modeled observed short-period Love and Rayleigh waves from a Texas quarry and found that the horizontal throw of material from the free face (spall model) is the dominant mechanism. Our MT analysis does not take into account the horizontal single-force component due to spall, the presence of tectonic prestress, the collapse of the quarry cliff face, and, for the production shot, the temporal and spatial spread from the delay-firing scheme. The duration of the ripple fire is around 500 ms where the typical delay between the boreholes is 16 ms. These complications contribute to the difficulty in obtaining unique source-type identification using long-period waveforms only (Fig. 8a). The nonisotropic component of the inversion results is manifested as a reverse mechanism with either a near-vertical or near-horizontal dipping layer and a vertical DS mechanism in the deviatoric solution. Because the short-period *P* waves may be more sensitive to radiated energy from the initial rupture (Pearce and Rogers, 1989; Guilhem *et al.*, 2014), including *P*-wave first-motion polarities is particularly useful to constrain the isotropic component of explosive events for which the first arrivals come from the detonated explosion. As illustrated in Figure 8, the added constraints from first-motion observations greatly reduces the ambiguity in source mechanism from waveforms and results in a unique identification of the events as having substantial volumetric components consistent with explosions.

MT-based event discrimination for shallow sources is reliable when SNR is high, especially with the combination of data from waveforms and first motions. When we include errors in the isotropic moment estimated from the NSS analysis, we see that although there is still a bias toward larger moment (events 800 and 400) even at such low yields and low magnitudes, the isotropic moments intersect with the empirical scaling relation. Although source inversions at greater depth reduce the effects of the free surface, in cases of extreme free-surface effects and complexities in the source such as the chemical explosions from this study, added errors from incorrect source depth can impact event discrimination. Incorrect source depth can result in biases up to a factor of 2 in the total seismic moment and isotropic moment based on the average values in our synthetic study (Fig. 4). Two other factors that are difficult to quantify can also contribute to the difference in our estimated yield and the design yield: one is the nature of the explosive, and the other is the frequency content of the waveforms used to derive the magnitude-yield scaling law. The Stevens and Murphy (2001) scaling law is derived from modeling large nuclear explosions at relatively long periods (17–60 s; Given and Mellman, 1986). For the same yield, nuclear explosions, single-fired buried chemical explosions, and ripple-fired quarry blasts exhibit differences in radiated seismic energy (Murphy, 1996); therefore, additional scaling is required to factor in the differences in seismic coupling for different types of explosions. All three shots are partially confined, but the production shot uses a ripple-firing scheme, and the two smaller shots are single-fired chemical explosions. Traditionally single-fired shots are designed to maximize the strength of the seismic signal (Khalturin *et al.*, 1998). In addition, possible site effect due to the use of short-period waveforms from temporary surface sensors may contribute to the overestimation of the yield.

Conclusions

Theoretical DS GFs have vanishing amplitudes near the free surface because the associated MT elements M_{xz} and M_{yz} radiate little seismic energy, whereas the GF waveforms look similar with little phase distortion. However, synthetic calculations at shallow depths show MT-based event discrimination is reliable, and the resolvability of the MT solution depends on station configuration, noise level, the period range, and the velocity model.

We are able to recover a predominantly explosive source mechanism for the three HUMMING ALBATROSS chemical explosions from MT inversions. Although the source-type uncertainty analysis shows that we cannot uniquely characterize the events as predominantly explosive using only waveform data, the combined waveform and first-motion method enables the unique discrimination of these events. This method has been applied in previous studies that have shown that the inclusion of *P*-wave first motions, in addition to full waveform data, eliminates the common ISO–CLVD trade-off (Ford *et al.*, 2012; Chiang *et al.*, 2014) and reduces the uncertainties of sparsely recorded underground explosions with strong Love waves and reversed Rayleigh waves (Chiang *et al.*, 2014). In this study, we further demonstrate that incorporating the two data sets is particularly useful in constraining the isotropic component of explosions, and the method applies not only to large events but also to small magnitude, very shallow explosions that are effectively at the free surface. The combination of both long-period full waveform data and short-period *P*-wave polarities greatly enhances the capabilities of the MT source-type discrimination method in cases of sparse station coverage, strong Love waves, and free-surface effects.

The MT method is capable of event discrimination. Although yield estimation using the recovered absolute seismic moment from MT inversion remains challenging and can have large uncertainties, we can begin to put error bounds on our moment estimates, and therefore yield, using the NSS technique and combining waveform and first motion. Pure explosion synthetic tests suggest that source inversions at deeper

depths reduce the free-surface effects on the moment, but we cannot draw definite conclusions using the results from the HUMMING ALBATROSS data set, due not only to free-surface effects but also to uncertainties associated with imperfect knowledge of the Earth structure, unaccounted nonisotropic radiation due to the mass movement of the quarry face, and differences in seismic coupling between different types of explosions. In addition, the moment–yield relationship derived from larger nuclear explosions may not be adequate for such low-magnitude chemical explosions.

Data and Resources

All seismic data were provided by Weston Geophysical Corp. Plots were made using the Generic Mapping Tools (GMT) v.4.5.8 (http://gmt.soest.hawaii.edu/, last accessed September 2014; Wessel and Smith, 1998), and MATLAB v.8.5.0.197613 (R2015a).

Acknowledgments

We acknowledge funding from the Air Force Research Laboratory, Contract Number FA9453-10-C-0263 that supported this research, and we thank Václav Vavryčuk and an anonymous reviewer for their comments and suggestions on the article. This work was performed under the auspices of the U.S. Department of Energy by Lawrence Livermore National Laboratory under Contract Number DE-AC52-07NA27344.

References

Barker, T. G., K. L. McLaughlin, J. L. Stevens, and S. M. Day (1993). Numerical models of quarry blast sources: Effects of the bench, *S-CUBED Report, SSS-TR-93–13915*.

Bonner, J. L, E. T. Herrin, and T. T. Goforth (1996). Azimuthal variation of *Rg* from central Texas quarry blasts, *Seismol. Res. Lett.* **67,** 43.

Bowers, D., and J. A. Hudson (1999). Defining the scalar moment of a seismic source with a general moment tensor, *Bull. Seismol. Soc. Am.* **89,** 1390–1394.

Bukchin, B., E. Clévédé, and A. Mostinskiy (2010). Uncertainty of moment tensor determination from surface wave analysis for shallow earthquakes, *J. Seismol.* **14,** 601–614.

Burger, R. W., T. Lay, T. C. Wallace, and L. J. Burdick (1986). Evidence of tectonic release in long-period *S* waves from underground nuclear explosions at the Novaya Zemlya test sites, *Bull. Seismol. Soc. Am.* **76,** 733–755.

Chiang, A., D. S. Dreger, S. R. Ford, and W. R. Walter (2014). Source characterization of underground explosions from combined regional moment tensor and first-motion analysis, *Bull. Seismol. Soc. Am.* **104,** no. 4, 1587–1600.

Dreger, D. S., S. R. Ford, and W. R. Walter (2008). Source analysis of the Crandall Canyon, Utah, mine collapse, *Science* **321,** 217.

Ekström, G., and P. G. Richards (1994). Empirical measurements of tectonic moment release in nuclear explosions from teleseismic surface waves and body waves, *Geophys. J. Int.* **117,** 120–140.

Ford, S. R., D. S. Dreger, and W. R. Walter (2008). Source characterization of the 6 August 2007 Crandall Canyon mine seismic event in central Utah, *Seismol. Res. Lett.* **79,** 637–644.

Ford, S. R., D. S. Dreger, and W. R. Walter (2009a). Source analysis of the Memorial Day explosion, Kimchaek, North Korea, *Geophys. Res. Lett.* **36,** L21304, doi: 10.1029/2009gl040003.

Ford, S. R., D. S. Dreger, and W. R. Walter (2009b). Identifying isotropic events using a regional moment tensor inversion, *J. Geophys. Res.* **114,** no. B01306, doi: 10.1029/2008JB005743.

Ford, S. R., D. S. Dreger, and W. R. Walter (2010). Network sensitivity solutions for regional moment-tensor inversions, *Bull. Seismol. Soc. Am.* **100,** 1962–1970.

Ford, S. R., W. R. Walter, and D. S. Dreger (2012). Event discrimination using regional moment tensors with teleseismic-*P* constraints, *Bull. Seismol. Soc. Am.* **102,** 867–872.

Given, J. W., and G. R. Mellman (1986). Estimating explosion and tectonic release source parameters of underground nuclear explosions from Rayleigh and Love wave observations, *Air Force Geophysics Laboratory Technical Report No. AFGL-TR-86-0171(I)*.

Goforth, T. T., and J. L. Bonner (1995). Characteristics of *Rg* waves recorded in central Texas, *Bull. Seismol. Soc. Am.* **85,** 1232–1235.

Guilhem, A., L. Hutchings, D. S. Dreger, and L. R. Johnson (2014). Moment tensor inversions of M ∼ 3 earthquakes in the Geysers geothermal fields, California, *J. Geophys. Res.* **119,** no. 3, doi: 10.1002/2013JB010271.

Herrmann, R. B. (2013). Computer programs in seismology: An evolving tool for instruction and research, *Seismol. Res. Lett.* **84,** no. 6, 1081–1088.

Herrmann, R. B., and C. Y. Wang (1985). A comparison of synthetic seismograms, *Bull. Seismol. Soc. Am.* **75,** no. 1, 41–56.

Hudson, J. A., R. G. Pearce, and R. M. Rogers (1989). Source type plot for inversion of the moment tensor, *J. Geophys. Res.* **94,** 765–774.

Jost, M. L., and R. B. Herrmann (1989). A student's guide to and review of moment tensors, *Seismol. Res. Lett.* **60,** no. 2, 37–57.

Julian, B. R., A. D. Miller, and G. R. Foulger (1998). Non-double-couple earthquakes 1. Theory, *Rev. Geophys.* **36,** no. 4, 525–549.

Khalturin, V. I., T. G. Rautian, and P. G. Richards (1998). The seismic signal strength of chemical explosions, *Bull. Seismol. Soc. Am.* **88,** no. 6, 1511–1524.

Knopoff, L., and M. J. Randall (1970). The compensated linear vector dipole: A possible mechanism for deep earthquakes, *J. Geophys. Res.* **75,** 4957–4963.

McLaughlin, K. L., J. L. Bonner, and T. Barker (2004). Seismic source mechanisms for quarry blasts: Modelling observed Rayleigh and Love wave radiation patterns from a Texas quarry, *Geophys. J. Int.* **156,** 79–93, doi: 10.1111/j.1365-246X.2004.02105.x.

McNamara, D. E., H. M. Benz, R. B. Herrmann, E. A. Bergman, P. Earle, A. Holland, R. Baldwin, and A. Gassner (2015). Earthquake hypocenters and focal mechanisms in central Oklahoma reveal a complex system of reactivated subsurface strike-slip faulting, *Geophys. Res. Lett.* **42,** no. 8, 2742–2749, doi: 10.1002/2014GL062730.

Minson, S. E., and D. S. Dreger (2008). Stable inversions for complete moment tensors, *Geophys. J. Int.* **174,** 585–592.

Minson, S. E., D. S. Dreger, R. Bürgmann, H. Kanamori, and K. M. Larson (2007). Seismically and geodetically determined nondouble-couple source mechanisms from the 2000 Miyakejima volcanic earthquake swarm, *J. Geophys. Res.* **112,** no. B10308, doi: 10.1029/2006JB004847.

Mueller, R. A., and J. R. Murphy (1971). Seismic characteristics of underground nuclear detonations, part I: Seismic spectrum scaling, *Bull. Seismol. Soc. Am.* **61,** 1675–1692.

Murphy, J. R. (1977). Seismic source functions and magnitude determinations for underground nuclear detonations, *Bull. Seismol. Soc. Am.* **67,** no. 1, 135–158.

Murphy, J. R. (1996). Types of seismic events and their source descriptions, in *Monitoring a Comprehensive Test Ban Treaty*, E. S. Husebye and A. M. Dainty (Editors), Kluwer Academic Publishers, Dordrecht, The Netherlands, 225–245.

Nayak, A., and D. S. Dreger (2015). Source-type specific inversion of moment tensors, *Bull. Seismol. Soc. Am.* **105,** no. 6, 2987–3000.

Patton, H. J. (2012). Modeling M_s-yield scaling of Nevada test site nuclear explosions for constraints on volumetric moment due to source-medium damage, *Bull. Seismol. Soc. Am.* **102,** no. 4, 1373–1387.

Pearce, R. G., and R. M. Rogers (1989). Determination of earthquake moment tensors from teleseismic relative amplitude observations, *J. Geophys. Res.* **94,** no. B1, 775–786.

Saikia, C. K., A. L. Kafka, S. C. Gnewuch, and J. W. Mctigue (1990). Shear velocity and intrinsic *Q* structure of the shallow crust in southeastern New England from *Rg* wave dispersion, *J. Geophys. Res.* **95,** no. B6, 8527–8541.

Song, X. J., D. V. Helmberger, and L. Zhao (1996). Broad-band modelling of regional seismograms: The basin and range crustal structure, *Geophys. J. Int.* **125,** no. 1, 15–29.

Stevens, J. L., and J. R. Murphy (2001). Yield estimation from surface-wave amplitudes, *Pure Appl. Geophys.* **158,** no. 11, 2227–2251.

Tape, W., and C. Tape (2012a). A geometric setting for moment tensors, *Geophys. J. Int.* **190,** no. 1, 476–498, doi: 10.1111/j.1365-246X.2012.05491.x.

Tape, W., and C. Tape (2012b). A geometric comparison of source-type plots for moment tensors, *Geophys. J. Int.* **190,** no. 1, 499–510, doi: 10.1111/j.1365-246X.2012.05490.x.

Templeton, D. C., and D. S. Dreger (2006). Non-double-couple earthquakes in the Long Valley volcanic region, *Bull. Seismol. Soc. Am.* **96,** no. 1, 69–79, doi: 10.1785/0120040206.

Vavryčuk, V. (2015). Moment tensor decompositions revisited, *J. Seismol.* **19,** no. 1, 231–252.

Vavryčuk, V., and S. G. Kim (2014). Nonisotropic radiation of the 2013 North Korean nuclear explosion, *Geophys. Res. Lett.* **41,** no. 20, 7048–7056, doi: 10.1002/2014GL061265.

Wang, C. Y., and R. B. Herrmann (1980). A numerical study of *P*-, *SV*-, and *SH*-wave generation in a plane layered medium, *Bull. Seismol. Soc. Am.* **70,** no. 4, 1015–1036.

Wessel, P., and W. H. F. Smith (1998). New, improved version of the generic mapping tools released, *Eos Trans. AGU* **79,** 579 pp.

Lawrence Livermore National Laboratory
7000 East Avenue
Livermore, California 94550
chiang4@llnl.gov
(A.C., S.R.F., W.R.W.)

Berkeley Seismological Laboratory
307 McCone Hall
Berkeley, California 94720
(D.S.D.)

Weston Geophysical Corp.
181 Bedford Street, Suite 1
Lexington, Massachusetts 02420
(S.-H.Y.)

Manuscript received 30 August 2015;
Published Online 11 October 2016